

# GEOMETRIC NONLINEAR ANALYSIS OF TWO-LAYER TIMBER COMPOSITE BEAMS WITH ELASTIC CONNECTIONS USING THE $\gamma$ -METHOD IN MATLAB

Le Thuy Nguyen<sup>1</sup>, \*Hong Son Nguyen<sup>2</sup> and Thuy Van Tran Thi<sup>3</sup>

<sup>1,2,3</sup>Faculty of Civil Engineering, Hanoi Architectural University, Vietnam

\*Corresponding Author, Received: 06 Nov. 2025, Revised: 23 Jan. 2026, Accepted: 30 Jan. 2026

**ABSTRACT:** In sustainable construction, two-layer composite timber beams with elastic shear connections are increasingly adopted due to their efficient use of material and enhanced structural performance. However, existing design procedures, such as the  $\gamma$ -method specified in EN 1995-1-1, are primarily based on linear assumptions and often neglect geometric nonlinearity. This simplification may lead to underestimation of deformation and stiffness reduction in slender composite members subjected to higher load levels. In this study, an enhanced numerical framework is developed in MATLAB to investigate the nonlinear behavior of two-layer composite timber beams. The proposed approach integrates a tangent-stiffness updating scheme with the von Kármán strain formulation, enabling consideration of geometric nonlinearity, including P- $\Delta$  effects and membrane forces. The numerical results demonstrate that geometric nonlinearity leads to a significant increase in mid-span deflection, ranging from 22% to 31% compared with linear analysis under advanced loading stages. In addition, the analysis identifies a critical connection stiffness threshold, beyond which the composite system approaches full interaction behavior. The proposed framework provides a practical and reliable computational tool for engineers, allowing more accurate assessment of deformation and stiffness characteristics and contributing to safer and more rational design of slender composite timber beams.

*Keywords: Timber Structures; Composite Timber Beam;  $\gamma$  - Method; Elastic-Shear Connection; MATLAB; Geometric Nonlinearity.*

## 1. INTRODUCTION

In the context of sustainable construction, composite timber members have gained increasing attention due to their lightweight nature, renewability, and low carbon emissions [1]. A key mechanical characteristic of such members lies in the elastic shear connection between layers, which possesses a finite shear stiffness ( $K$ ). This finite stiffness allows partial slip between layers, resulting in partial interaction behaviour [2]. The accurate characterization of the effective bending stiffness and serviceability deflection of composite timber beams directly depends on the connection parameters, including the shear modulus, shear stiffness, fastener spacing, and composite configuration [3, 4].

The standard EN 1995-1-1 introduces a simplified approach for mechanically jointed composite beams, presented in Annex B (Mechanically jointed beams). This method employs a coefficient  $\gamma$  to calculate the effective bending stiffness of sections with partial interaction. In technical literature and research, the calculation approach described in Annex B is commonly referred to as the “gamma ( $\gamma$ ) method” [5–7]. Owing to its simple formulation, clear mechanical interpretation, and close consistency with code provisions, the  $\gamma$ -method has become a widely accepted reference framework for evaluating serviceability deflection and comparing connection

alternatives in design [6, 7].

However, most applications of the  $\gamma$ -method in engineering practice have been limited to linear elastic analysis [8]. For slender beams or in cases where the boundary conditions restrict longitudinal displacement, accounting for geometric nonlinearity according to the von Kármán (P- $\Delta$ ) theory leads to significant differences in results: lateral deformation induces axial membrane forces, which in turn alter the tangent stiffness and cause the load-deflection curve to deviate depending on the load level [9–11]. Although finite element simulations can be used to describe this phenomenon, such approaches require complete material and connection data, involve high computational complexity, and demand considerable analysis time, which makes them unsuitable for rapid parametric studies or preliminary design [12–14].

In this paper, the authors propose a MATLAB-based analytical procedure for two-layer composite timber beams with elastic shear connections (finite slip stiffness), developed on the basis of the  $\gamma$ -method [5] and extended to account for geometric nonlinearity using a tangent-stiffness updating scheme. The procedure consists of several steps. The Euler–Bernoulli beam problem is subsequently solved using the finite element method, where the geometric stiffness matrix is derived from axial membrane forces estimated from the rotation field. Finally, the analysis establishes the load-deflection

curve, the evolution of membrane forces, the tangent stiffness, the nonlinearity index (defined as the ratio of nonlinear to linear response), and parametric maps with respect to span length  $L$ , timber layer thickness  $t$ , and connection stiffness  $K$  [12, 14, 15].

Experimental and numerical data are used to verify and calibrate the connection stiffness  $K$ , ensuring the practical reliability of the model while keeping it compact, transparent, and easily reproducible [16, 17].

Despite the popularity of the  $\gamma$ -method for its simplicity, it is primarily based on first-order linear elastic theory. As noted by [18], the assumption of small displacements may not hold for slender composite beams or those subjected to significant axial constraints. In such cases, geometric nonlinearity specifically the  $P-\Delta$  effect becomes a dominant factor in structural response. Recent studies in the International Journal of GEOMATE have highlighted the sensitivity of composite systems to connection efficiency [19] and the need for advanced numerical verification [20].

The primary justification for considering geometric nonlinearity in this study lies in the "membrane effect" generated by global longitudinal restraints. When the beam undergoes large deflections, the internal membrane force significantly alters the tangent stiffness. This phenomenon is often overlooked in conventional timber design but is critical for preventing premature serviceability failure. This paper fills this gap by providing a MATLAB-based FEA tool that reconciles the practical  $\gamma$ -method with rigorous second-order analysis.

The aim of this study is to demonstrate that, although much simpler than detailed finite element analysis, the  $\gamma$ -based procedure can reproduce the main mechanical characteristics of composite timber beams within the serviceability range considering geometric nonlinearity, while providing a set of graphical results that enable comparison of connection alternatives and support design decisions.

## 2. RESEARCH SIGNIFICANCE

This study addresses a practical limitation in the design of two-layer composite timber beams with elastic shear connections, where geometric nonlinearity is commonly neglected in standard applications of the  $\gamma$ -method in EN 1995-1-1. An enhanced MATLAB-based framework is proposed by integrating von Kármán geometric nonlinearity into a tangent-stiffness updating scheme. The approach enables efficient consideration of  $P-\Delta$  effects and membrane forces while retaining the simplicity of design-oriented calculations. The results provide engineers with a practical tool for more accurate deformation assessment and rational design of slender composite timber beams.

## 3. THEORETICAL BACKGROUND AND ANALYSIS METHOD

### 3.1. Mechanical Model and Assumptions

The  $\gamma$ -method presented in Annex B of Eurocode 5 provides a simplified approach to transform a two-layer composite timber system connected by an elastic shear connection into an equivalent single-material beam with an effective bending stiffness  $EI_{\text{eff}}$ .

In practical structures, the connection between the two layers is rarely perfectly rigid and can transmit only part of the shear stress, resulting in relative slip and partial interaction between the layers. The main assumptions are as follows:

- The timber material behaves elastically with a modulus of elasticity  $E$ .

- Material: The composite timber beam consists of two layers, each having dimensions  $b \times t$  and span length  $L$ . The timber is assumed to be orthotropic, working in the serviceability range under linear elastic behavior with a longitudinal modulus of elasticity  $E$ . The cross-sectional area of each layer is  $A = b \cdot t$ , the second moment of area is  $I = bt^3/12$ , and the distance from the centroid of each layer to the neutral axis is  $a = t/2$ .

- Connection between layers: The layers are connected through an elastic shear connection characterized by a shear stiffness per unit length  $K$  (N/mm). The stiffness  $K$  is derived from the serviceability shear modulus of the fasteners  $K_{\text{ser}}$  (N/mm) considering the fastener spacing  $s$  (mm) along the beam axis and the number of fastener rows  $n_r$  as shown in Fig. 1.

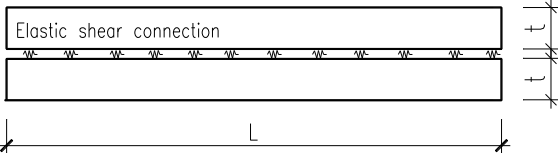
$$K \approx \frac{n_r \cdot K_{\text{ser}}}{s} \quad (1)$$


Fig. 1 Two-Layer Timber Composite Beam

- Bending assumption: The beam is modeled as an Euler-Bernoulli beam, neglecting shear deformation within each layer (valid for sufficiently large  $L/t$  ratios), with partial interaction between layers due to the finite shear stiffness  $K$ .

- Nonlinearity: Both the material and the connection behave elastically; geometric nonlinearity of the von Kármán type ( $P-\Delta$ ) is considered.

- Boundary conditions and loading: The beam is simply supported at both ends, with  $\omega(0) = \omega(L) = 0$  and free rotation at the supports. To activate the  $P-\Delta$  effect, the overall axial shortening of the system is constrained (global longitudinal restraint). The bending load is applied through a four-point loading configuration, with two equal loads positioned at  $L/3$

and  $2L/3$  along the span as shown in Fig.2.

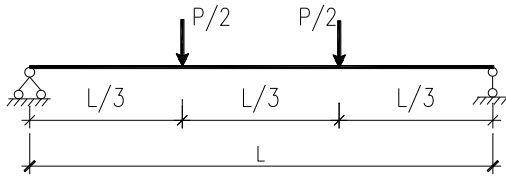


Fig. 2 Analysis scheme and four-point-loading configuration

### 3.2. Gamma Method and effective bending stiffness

#### 3.2.1. Limiting cases and effective bending stiffness

- The bending stiffness of a two-layer system lies between two limiting cases:

$$-EI_{nc} = E \cdot 2I \text{ (soft connection)}$$

$$-EI_{fc} = E \cdot [2 \cdot (I + A \cdot a^2)] \text{ (fully rigid connection)}$$

The actual behavior of the composite beam lies between these limits and is characterized by the coefficient  $\gamma$  ( $0 < \gamma < 1$ ), which reduces the coupling term  $E A a^2$  according to the degree of connection [5]:

$$\gamma = \frac{1}{1 + \pi^2 \frac{EA}{KL^2}} \quad (2)$$

The coefficient  $\gamma$  depends on the ratio between the axial stiffness  $EA/L^2$  and the shear stiffness  $K$ . When  $K$  is large or  $L$  is short,  $\gamma \rightarrow 1$  (fully composite); conversely, when  $K$  is small or  $L$  is long,  $\gamma \rightarrow 0$  (non-composite).

Accordingly, (3) give the effective bending stiffness [5]:

$$EI_{eff} = E \cdot 2I + 2 \cdot \gamma E A a^2 \quad (3)$$

To compare the degree of composite action among different connection configurations, a normalized connection efficiency index can be used:

$$\eta = \frac{EI_{eff} - EI_{nc}}{EI_{fc} - EI_{nc}} \in [0, 1], \quad (4)$$

where  $\eta = 1$  corresponds to a fully rigid connection, and  $\eta = 0$  corresponds to a soft connection. The origin of the expression defining the  $\gamma$  coefficient can be explained from the differential equation describing the relative slip between the two layers [5]. Consider two layers with longitudinal displacements  $u_1(x)$  and  $u_2(x)$ , and deflection  $\omega(x)$ . The relative slip is:

$$\delta(x) = u_1(x) - u_2(x) - 2a \frac{d\omega}{dx} \quad (5)$$

The distributed shear force in the connection is  $q(x) = K \cdot \delta(x)$ . From the equilibrium of axial forces in each layer:

$$EA \frac{d^2 u_1}{dx^2} = q(x), \quad EA \frac{d^2 u_2}{dx^2} = -q(x) \quad (6)$$

one obtains the governing equation for  $\delta(x)$ :

$$EA \frac{d^2 \delta}{dx^2} - 2K \cdot \delta = 0 \quad (7)$$

Solving this equation with boundary conditions  $\delta(0) = \delta(L) = 0$  and a sinusoidal bending moment distribution  $M(x) = M_0 \cdot \sin(\pi x/L)$  yields the slip function  $\delta(x)$ . Substituting it into the equation leads to the dimensionless parameter  $\pi^2 EA/(KL^2)$ , which represents the ratio between axial stiffness and shear stiffness.

The constant  $\pi$  appears due to the sinusoidal distribution of slip in a simply supported beam (first vibration mode). When formulating the global moment–curvature relationship, the coupling term  $E A a^2$  is reduced by a factor  $\left(1 + \pi^2 \frac{EA}{KL^2}\right)^{-1}$ , it means that  $\gamma$  as defined in Annex B of [5].

Therefore, the parameter  $\pi^2 EA/(KL^2)$  has the following physical interpretation:

+ When the parameter is large  $\rightarrow$  soft connection, large slip, small  $\gamma$ ;

+ When the parameter is small  $\rightarrow$  stiff connection, small slip,  $\gamma$  approaches 1.

#### 3.2.2. Application in bending analysis

In all linear bending equations (Euler–Bernoulli theory), the bending stiffness  $EI$  can be replaced by the effective stiffness  $EI_{eff}$  to determine deflection, rotation, or stress.

For example, for a simply supported beam under a uniformly distributed load  $q$ :

$$\delta_{max} = \frac{5qL^4}{384(EI)_{eff}} \quad (8)$$

By using the  $\gamma$ -method, the influence of the shear connection stiffness  $K$  on serviceability deflection and the degree of composite action can be quickly evaluated without solving complex differential equations.

Notes: It can thus be observed that the  $\gamma$ -method results from the analytical solution of the bending problem of a composite beam with an elastic shear connection, which has been standardized in [5] as a set of simplified expressions (Annex B) for the design of composite timber beams. This method accurately represents the partial interaction behavior of elastic connections and serves as a foundation for the development of more advanced analytical approaches.

### 3.3. Geometric Nonlinearity According to von Kármán (P–Δ)

#### 3.3.1. Scope and assumptions

The geometric nonlinear analysis considered here applies to cases of small strains but moderate rotations or deflections. The von Kármán

approximation is adopted for the Euler–Bernoulli beam with the following assumptions:

- Shear deformation within each layer is neglected.
- Both the material and the interlayer connection behave elastically (only geometric nonlinearity is considered).

### 3.3.2 von Kármán strain for the Euler–Bernoulli beam

For the lateral displacement  $\omega(x)$  (deflection) and the axial displacement  $u(x)$  of the neutral axis, the generalized axial strain (in the reduced Green–Lagrange form) at a fiber located a distance  $z$  from the neutral axis is expressed as:

$$\varepsilon(x, z) \approx u'(x) + \frac{1}{2}(\omega'(x))^2 - z\omega''(x) \quad (9)$$

where  $k(x) = \omega''(x)$  is the curvature of the neutral axis (sign convention according to bending),  $\theta(x) = \omega'(x)$  is the rotation of the cross-section. The nonlinear geometric component lies in the quadratic term  $\frac{1}{2}(\omega')^2$ , which induces axial membrane forces in the neutral axis even in the absence of external axial loading.

### 3.3.3. Axial membrane force and boundary constraint

The average axial force over the cross-section is given by [16, 20]:

$$N(x) = \int_A E \cdot \varepsilon(x, z) dA \approx EA_{eff} \left( u'(x) + \frac{1}{2} \cdot (\omega'(x))^2 \right) \quad (10)$$

since  $\int_A z dA = 0$  along the neutral axis.

In this study, the support–loading case corresponds to a simply supported beam with an overall longitudinal restraint. Accordingly, the boundary condition of zero total axial elongation along the span is applied.

$$\frac{1}{L} \int_0^L u'(x) dx \approx 0 \rightarrow \bar{\varepsilon}_0 \equiv \frac{1}{L} \int_0^L (u'(x) + \frac{1}{2} \theta^2(x)) dx \quad (11)$$

$$\approx \frac{1}{2L} \int_0^L \theta^2(x) dx$$

As a result, a self-induced membrane force  $N_{mem}$  arises due to geometry [9-11]:

$$N_{mem} = EA_{eff} \bar{\varepsilon}_0 = \frac{EA_{eff}}{2L} \int_0^L (\theta(x))^2 dx \geq 0 \quad (12)$$

It is observed that as deflection increases, the rotation  $\theta$  also increases, leading to accumulated geometric elongation. Consequently, a positive membrane force develops, increasing the tangent stiffness of the system, a “stiffening” type P– $\Delta$  effect within the serviceability range. In cases with initial compression or external axial force, the sign and magnitude of  $N$  may differ; however, in this study, only the case without external axial loading is

considered.

### 3.3.4. Equilibrium equation and “geometric stiffness”

In the Euler–Bernoulli beam model, the bending moment obeys a linear elastic law. The response is characterized by an effective bending stiffness.

$$M(x) = EI_{eff} k(x) = EI_{eff} \omega''(x) \quad (13)$$

When a membrane force  $N_{mem}$  exists, the tangent linearized transverse equilibrium equation becomes:

$$EI_{eff} \omega''''(x) + N_{mem} \cdot \omega''(x) = q(x) \quad (14)$$

where  $q(x)$  is the equivalent distributed or converted concentrated load [9, 10].

Eq. (14) represents the tangent linearization of the geometrically nonlinear beam problem according to von Kármán [9-11]. The term  $N_{mem} \cdot \omega''(x)$  is the origin of the geometric stiffness matrix, which modifies the tangent stiffness depending on the current deflection state.

For an element of length  $l_e$ , assuming linear interpolation of  $\theta$ . Under this assumption, the conventional form of the geometric stiffness matrix  $K_g$  can be expressed as [9-11]:

$$K_g = \frac{N_{mem}}{30 \cdot l_e} \begin{bmatrix} 36 & 3l_e & -36 & 3l_e \\ 3l_e & 4l_e^2 & -3l_e & -l_e^2 \\ -36 & -3l_e & 36 & -3l_e \\ 3l_e & -l_e^2 & -3l_e & 4l_e^2 \end{bmatrix} \quad (15)$$

In the two-node Euler–Bernoulli beam element (four degrees of freedom:  $\omega_1, \theta_1, \omega_2, \theta_2$ ), the linear bending stiffness matrix is [9-11]:

$$K_b = \frac{EI_{eff}}{l_e^3} \begin{bmatrix} 12 & 6l_e & -12 & 6l_e \\ 6l_e & 4l_e^2 & -6l_e & -2l_e^2 \\ -12 & -6l_e & 12 & -6l_e \\ 6l_e & -2l_e^2 & -6l_e & 4l_e^2 \end{bmatrix} \quad (16)$$

where  $l_e$  is the element length and  $EI_{eff}$  is the effective bending stiffness determined by the  $\gamma$ -method.

When considering geometric nonlinearity (P– $\Delta$ ), the total tangent stiffness matrix is obtained by summing the two matrices:

$$K_t = K_b + K_g \quad (17)$$

## 3.4. Analysis procedure using MATLAB

Based on the theoretical background presented in Sections 2.1–2.3, the authors developed a computational model in MATLAB to simulate the bending behavior of a two-layer glued laminated timber beam with elastic shear connection, taking into account geometric nonlinearity according to the von Kármán theory. The model was formulated using the

finite element method, with Euler–Bernoulli beam elements that include two degrees of freedom at each node as shown in Fig. 3.

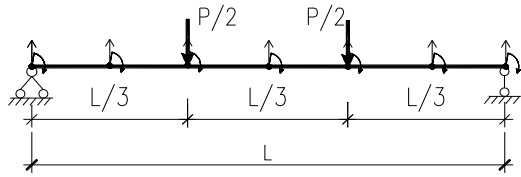


Fig. 3. Discretization of the beam and associated degrees of freedom

a. Input Data Definition

The geometric parameters  $b$ ,  $t$ ,  $L$ , the material modulus  $E$ , and the connection stiffness  $K$  are defined as input data.

The beam is divided into  $n_e$  finite elements (two-node Euler–Bernoulli elements with four degrees of freedom). Boundary conditions are specified as simply supported with no overall axial deformation. The load is applied incrementally in  $n_{step}$ , distributed at two positions,  $L/3$  and  $2L/3$ .

b. Calculation of Effective Parameters

From the material and connection properties, the composite interaction coefficient  $\gamma$  and the effective bending stiffness  $EI_{eff}$  are determined using the  $\gamma$ -method. These values are then assigned to the linear bending stiffness matrix  $\mathbf{K}_b$  and used in the nonlinear computation.

c. Assembly of the Stiffness Matrix

The element stiffness matrices are formulated and assembled into the global bending stiffness matrix  $[\mathbf{K}_b]$ . The displacement vector  $\{\mathbf{U}\}=0$  and the load vector  $\{\mathbf{F}\}$  are initialized.

At this stage, nonlinearity is not yet considered, and the system is in a purely elastic state.

d. Incremental Solution and Update of Axial Forces

The load is gradually increased from 0 to  $P_{max}$ . At each load step, the current displacements and rotations are used to compute the axial membrane force  $N_{mem}$  according to the expression (10) given in Section 2.3. This value is incorporated into the geometric stiffness matrix  $\mathbf{K}_g$  to update the tangent stiffness matrix as  $\mathbf{K}_t = \mathbf{K}_b + \mathbf{K}_g$ .

The incremental equilibrium equation  $\mathbf{K}_t \cdot \Delta \mathbf{U} = \Delta \mathbf{F}$  is solved for the system's degrees of freedom, and the displacements are accumulated for the next load step.

e. Updating and Convergence Check

After each iteration, the displacement vector  $\{\mathbf{U}\}$  is updated, and the displacement error  $\|\Delta \mathbf{U}\|$  is compared with the convergence tolerance. If the error exceeds the limit, the load increment is reduced or the number of Newton–Raphson iterations is increased for the current load step.

The procedure continues until the target load or deflection limit is reached.

f. Output and Post-Processing

Upon completion of the analysis, the program automatically generates plots, including the load–deflection ( $P$ – $\delta$ ) curves for both linear and nonlinear cases, the distribution of axial forces  $N_{mem}$ , the tangent stiffness  $K_t(P)$ , and the nonlinearity index  $\varphi = \delta_{non} / \delta_{lin}$ . The results are normalized and represented as parameter maps of  $\delta_{non}/L$  versus  $K$ ,  $L$ , and for parametric evaluation.

To ensure the numerical stability and accuracy of the proposed procedure, a mesh convergence study was conducted. The number of elements ( $n_{el}$ ) was varied from 10 to 80. It was observed that the mid-span deflection converged at  $n_{el} = 40$ , with a relative difference of less than 0.5% compared to finer meshes. Consequently, a mesh of 40 elements was adopted for all subsequent simulations to balance accuracy and computational cost.

## 4. RESULTS AND DISCUSSION

### 4.1 Input Parameters and Validation

To illustrate the computational procedure described in the previous sections, a two-layer timber composite beam subjected to symmetric four-point bending under simply supported conditions is considered. This loading configuration is commonly used in experiments to determine deflection and to validate bending models. The example is performed for a two-layer glued laminated timber beam with elastic–slip connection, evaluated using the  $\gamma$ -method of Eurocode 5, Annex B. The beam is simply supported and loaded at four symmetric points, and geometric nonlinearity ( $P$ – $\Delta$  effect) is activated by imposing zero overall axial deformation along the span (Fig. 4).

Geometric and material parameters: Span  $L=2.4\text{m}$ ; width of each layer  $b=60\text{mm}$ ; thickness  $t=30\text{mm}$ ; elastic modulus  $E=11000\text{MPa}$ ; shear stiffness  $K=600\text{N/mm}$ . The load consists of two concentrated forces  $P/2$  applied at  $L/3$  and  $2L/3$ . The beam is discretized into 40 two-node Euler–Bernoulli elements (four degrees of freedom per element).

Analysis: The computations are performed in MATLAB using an in-house code, and two cases are compared:

- Linear elastic analysis (without  $P$ – $\Delta$  effects);
- Geometric nonlinear analysis including self-induced membrane forces.

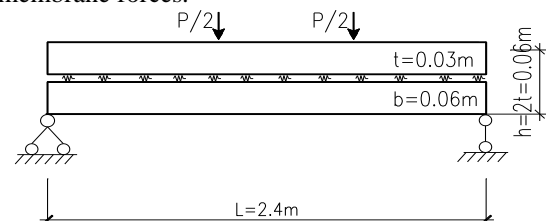


Fig. 4. Case Study: Bending Analysis of a Two-Layer Timber Composite Beam

The effective bending stiffness  $EI_{\text{eff}}$  is evaluated via the  $\gamma$ -method and assigned to the element stiffness matrices. The global tangent stiffness is updated iteratively using the Newton–Raphson procedure until convergence is achieved.

The linear results obtained from the MATLAB procedure show perfect agreement with the analytical  $\gamma$ -method specified in EN 1995-1-1 for low load levels, verifying the baseline accuracy of the numerical model.

#### 4.2 Nonlinear Behavior and Parametric Study

Using the developed MATLAB framework, the numerical results are reported and discussed in the following subsections.

##### 4.2.1 Load–deflection relationship ( $P-\delta$ )

The results indicate that the  $P-\delta$  curve of the geometrically nonlinear beam. In the initial stage, the two curves nearly coincide, demonstrating that the initial elastic stiffness is captured accurately. As the load increases, second-order effects become apparent, reducing the stiffness and causing the nonlinear  $P-\delta$  curve to bend more noticeably.

At higher load levels, approaching approximately 80–90% of the maximum applied load, the nonlinear deflection exceeds the linear prediction by about 20–30%, depending on the beam slenderness and connection stiffness. This deformation amplification is attributed to second-order ( $P-\Delta$ ) effects, in which self-induced axial membrane forces progressively reduce the tangent stiffness and amplify lateral deflections. These findings emphasize the necessity of considering geometric nonlinearity when analyzing slender beams or beams subjected to near-limit loading, in order to achieve more accurate predictions of deflection and structural stability.

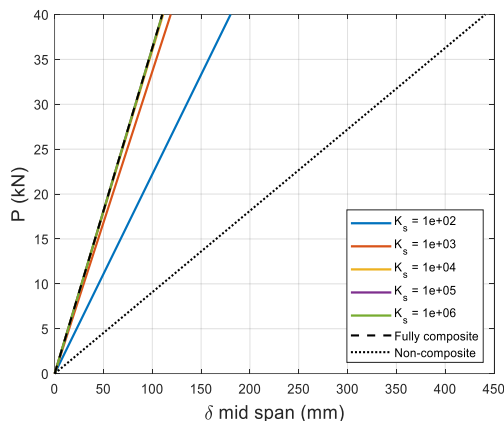


Fig. 5. Influence of shear-connection stiffness  $K_s$  on the load–deflection response

##### 4.2.2 Influence of the shear connection stiffness $K_s$ on the effectiveness of composite action

Fig. 6 illustrates the relationship between the shear-connection stiffness  $K_s$  and the composite-action efficiency  $\eta$ , which characterizes the degree of cooperative action between the layers in a multi-layer composite beam. Here,  $K_s$  represents the shear stiffness of the slip connection between the two layers.

As  $K_s$  increases from  $10^2$  to  $10^4$  N/mm<sup>2</sup>, the efficiency  $\eta$  rises rapidly from approximately 0.45 to nearly 1.0, indicating a significant improvement in the interlayer shear interaction. When  $K_s \geq 10^5$  N/mm<sup>2</sup>,  $\eta$  approaches its maximum value, corresponding to a fully composite state in which the two layers behave as a single structural unit.

These results show that the shear-connection stiffness plays a decisive role in the overall composite efficiency: when  $K_s$  is low, the beam exhibits only partial composite action, resulting in a reduced bending stiffness; in contrast, sufficiently large  $K_s$  provides stiffness levels close to those of a fully composite member. Therefore, in the design of multi-layer composite beams, a minimum shear-connection stiffness of approximately  $10^4$  N/mm<sup>2</sup> is recommended to ensure the desired level of composite action.

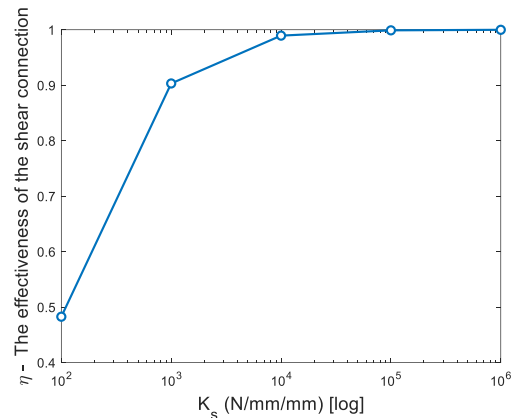


Fig. 6. Influence of shear-connection stiffness  $K_s$  on the load–deflection response

##### 4.2.3 Influence of the shear connection stiffness $K_s$ on the effectiveness of composite action

Fig. 7 shows that the  $P-\delta$  curve of the geometrically nonlinear beam exhibits a pronounced downward curvature compared with the linear reference response, clearly reflecting the influence of second-order ( $P-\Delta$ ) effects. In the low-load range, the two curves nearly coincide, indicating that the initial elastic stiffness is accurately captured. However, as the load increases, the tangent stiffness gradually decreases, causing the nonlinear curve to bend more sharply and the deflection to grow rapidly.

At higher load levels, the discrepancy between the two models becomes significant: the nonlinear deflection may exceed the linear prediction by 20–30%, indicating the gradual loss of stiffness and stability due to geometric effects. These results confirm that geometric nonlinearity must be

considered when analyzing slender beams or beams subjected to near-limit loading, in order to achieve accurate predictions of displacement and overall stability.

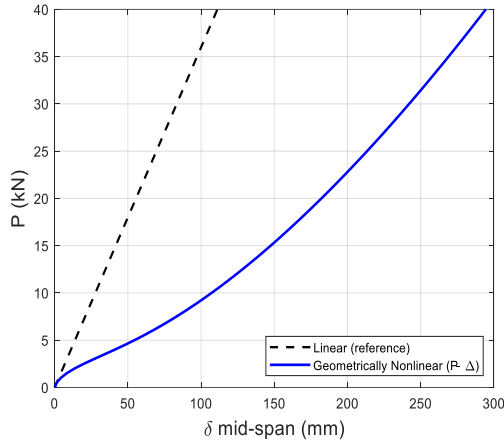


Fig. 7. Load-deflection  $P$ - $\delta$  curves for linear and geometrically nonlinear analyses

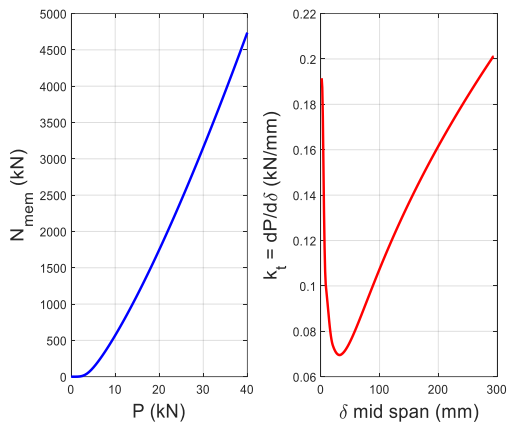


Fig. 8. Membrane-force development and tangent-stiffness reduction due to geometric nonlinearity

4.2.4 Development of second-order membrane force and corresponding tangent stiffness of the beam

Fig. 8 presents the evolution of the membrane force  $N_{mem}$  with respect to the applied load  $P$  (left), and the variation of the tangent stiffness  $k_t=dP/d\delta$  with midspan deflection  $\delta$  (right). The results show that the membrane force increases nonlinearly with load, demonstrating the pronounced influence of the  $P$ - $\Delta$  effect in the large-deflection range. The increasing curvature of the  $N_{mem}$ - $P$  curve indicates that the internal force develops faster than the nominal load, a characteristic feature of geometric-induced secondary effects.

The  $k_t$ - $\delta$  plot shows that the tangent stiffness decreases sharply at the initial stage from approximately 0.20 to 0.07 kN/mm when  $\delta < 100$  mm indicating a rapid loss of initial stiffness. Beyond this point, the curve gradually rises and stabilizes around 0.20 kN/mm, reflecting a redistribution of internal forces as the structure approaches a new

geometrically compatible equilibrium. This behavior is consistent with the mechanics of geometric nonlinearity, in which the stiffness initially softens due to large deformations and subsequently increases slightly as the deformed shape becomes “stretched” under higher loads.

Overall, the results confirm that the beam is significantly affected by geometric nonlinearity and second-order effects, highlighting the need for analysis models that account for stiffness variation with displacement to accurately capture structural stability and realistic deflection behavior.

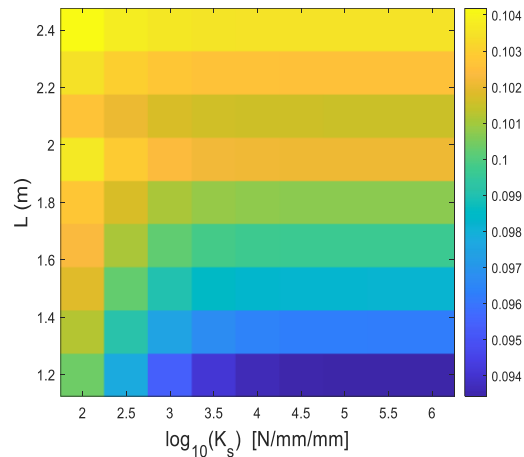


Fig. 9. Effective bending stiffness distribution with respect to  $L$  and  $K_s$

4.2.5 Combined influence of shear-connection stiffness and beam length

The two figures illustrate the combined influence of the shear-connection stiffness  $K_s$  and the beam length  $L$  on the key response quantities of the composite beam. In Fig.9, the color variation changes only mildly along both axes, indicating that the investigated quantity (e.g., equivalent bending stiffness or composite-action efficiency  $\eta$ ) increases gradually with increasing  $K_s$  and  $L$ , but with relatively low sensitivity.

When  $K_s$  is sufficiently large ( $\geq 10^4 N/mm^2$ ), the results approach a saturated value, implying that the slip connection becomes stiff enough to ensure nearly full composite action, with negligible dependence on the beam length.

In contrast, Fig.10 shows a much more pronounced variation: the response quantity increases significantly when  $L$  decreases or  $K_s$  increases, indicating that deflection and geometric sensitivity are substantially reduced for stiffer connections or shorter beams.

This confirms that, in practical design, both parameters  $L$  and  $K_s$  play important roles in governing the overall behavior: Longer beams  $\rightarrow$  stronger geometric nonlinearity; Softer connections  $\rightarrow$  reduced composite efficiency and increased deflection.

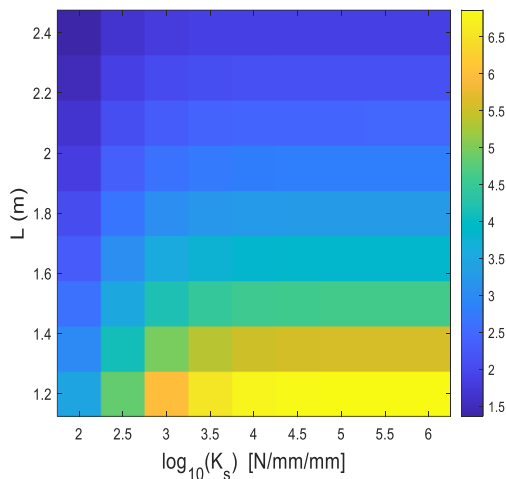


Fig. 10 Heatmap of composite-action coefficient  $\eta$  versus beam length  $L$  and shear stiffness  $K_s$

## 5. CONCLUSIONS

The analysis results show that the behavior of the composite beam is strongly influenced by geometric nonlinearity and the shear-connection stiffness between layers. The load–deflection ( $P$ – $\delta$ ) response reveals that the  $P$ – $\Delta$  effect significantly reduces stiffness as the load increases, causing the actual deflection to exceed the linear prediction by 20–30%.

The composite-action coefficient  $\eta$  and the equivalent bending stiffness  $EI_{\text{eff}}$  increase rapidly with the shear-connection stiffness  $K_s$ ; when  $K_s \geq 10^4$  N/mm<sup>2</sup>, the beam approaches a fully composite state, whereas for  $K_s < 10^3$  N/mm<sup>2</sup>, interlayer slip leads to a substantial reduction in the global stiffness. At the same time, the beam length  $L$  has a clear influence: longer beams exhibit stronger geometric nonlinear effects and greater sensitivity to  $K_s$ .

The results for bending moment and tangent stiffness indicate that the system stiffness decreases rapidly at the initial loading stage and then gradually stabilizes as a new geometric equilibrium is reached. The  $L$ – $K_s$  heatmaps further confirm these trends, showing that short beams with stiff shear connections provide the highest mechanical efficiency.

Overall, the study demonstrates that accounting for both geometric nonlinearity and slip-connection characteristics is essential for accurately predicting the behavior of composite beams. The findings also provide practical guidance for determining the minimum required shear-connection stiffness and permissible beam lengths in structural design.

## 6. REFERENCES

- Brandner R., Frangiaco M., & Schickhofer G., Performance of mechanically jointed timber members under serviceability loading, *European Journal of Wood and Wood Products*, Vol. 74, Issue 5, 2016, pp. 789–803.
- Fragiacomo M., & Lukaszewicz A., Slip modulus of mechanical fasteners in timber composites, *Construction and Building Materials*, Vol. 152, pp. 660–672.
- Lukaszewicz A., Partial composite action in timber beams, *Engineering Structures*, Vol. 110, pp. 155–165. DOI: 10.1016/j.engstruct.2016.02.048.
- Smith I., Deflection prediction of multi-layer timber beams, *European Journal of Wood and Wood Products*, Vol. 76. DOI: 10.1007/s00107-017-1180-5.
- EN 1995-1-1: Eurocode 5 – Design of Timber Structures – Part 1–1. CEN, Brussels, 2004, pp 01-123.
- Dias A., Mechanically jointed timber beams, *Construction and Building Materials*, Vol. 212, 2019, pp. 447–457.
- Yeoh D., Fragiaco M., Revisiting the  $\gamma$ -method for composite timber members, *Journal of Structural Engineering*, Vol. 146, Issue 9, 2020, pp. 01-12.
- Lam F., & Jeong G.Y., Behaviour of composite timber beams with partial interaction, *Journal of Structural Engineering*, Vol. 143, Issue, 2017, pp. 01-11. DOI: 10.1061/(ASCE)ST.1943-541X.0001650.
- Crisfield M., *Non-linear Finite Element Analysis of Solids and Structures*, Wiley, 1991, pp. 01-345.
- Reddy, J. N., *Energy Principles and Variational Methods in Structural Mechanics*, 2017, pp.01-592.
- Shabana A., Geometric nonlinearity in beam-type structures, *Nonlinear Dynamics*, Issue 95, 2019, pp.773-794.
- D’Amico B., & Frangi A., Analytical modelling of composite timber beams, *Journal of Construction and Building Materials*, 2019, pp. 01-229.
- Rajčić V., FEM modelling of timber composite beams with slip connections, *Composite Structures*, 2020, pp. 01-235.
- Hassanieh A., Efficient computational models for composite timber beams with partial interaction, *Journal of Building Engineering*, Vol. 32, 2020, pp. 01-15.
- O’Neill C., & Broughton, J., Experimental study of two-layer timber composite beams, *Construction and Building Materials*, Vol. 123, 2016, pp.145-158.
- Brandner R., Timber composite joints: performance and stiffness, *European Journal of Wood and Wood Products*, Vol. 76, 2018, pp. 341-353. DOI: 10.1007/s00107-017-1201-z.
- Nocetti M., Timber composite systems with elastic shear connectors: modelling and performance, *Structures*, Vol. 52, 2024, pp. 784–798. DOI: 10.1016/j.istruc.2024.12.005.
- Thin N., and Anh N., Numerical analysis of

- structural behavior of composite beams using sustainable materials, *International Journal of GEOMATE*, Vol. 24, Issue 102, 2023, pp.55-62.
19. Sato K., Influence of connection stiffness on the long-term deformation of timber structures, *International Journal of GEOMATE*, Vol.26,

Issue 115, 2024, pp. 10-18.

---

Copyright © Int. J. of GEOMATE All rights reserved, including making copies, unless permission is obtained from the copyright proprietors.

---